Metabolomics (2012) 8:930–939
DOI 10.1007/s11306-011-0388-y

ORIGINAL ARTICLE

High information throughput analysis of nucleotides and their isotopically enriched isotopologues by direct-infusion FTICR-MS

Pawel Lorkiewicz · Richard M. Higashi · Andrew N. Lane · Teresa W.-M. Fan

Received: 23 September 2011 / Accepted: 23 November 2011 / Published online: 9 December 2011

Abstract Fourier transform-ion cyclotron resonance-mass spectrometry (FTICR-MS) is capable of acquiring unmatched quality of isotopologue data for stable isotope resolved metabolomics (SIRM). This capability drives the need for a continuous ion introduction for obtaining optimal isotope ratios. Here we report the simultaneous analysis of mono and dinucleotides from crude polar extracts by FTICR-MS by adapting an ion-pairing sample preparation method for LC–MS analysis. This involves a rapid cleanup of extracted nucleotides on pipet tips containing a C_{18} stationary phase, which enabled global analysis of nucleotides and their ^{13}C isotopologues at nanomolar concentrations by direct infusion nanoelectrospray FTICR-MS with 5 min of data acquisition. The resolution and mass accuracy enabled computer-assisted unambiguous assignment of most nucleotide species, including all phosphorylated forms of the adenine, guanine, uracil and cytosine nucleotides, NAD^+, NADH, $NADP^+$, NADPH, cyclic nucleotides, several UDP-hexoses, and all their ^{13}C isotopologues. The method was applied to a SIRM study on human lung adenocarcinoma A549 cells grown in [U-^{13}C] glucose with or without the anti-cancer agent methylseleninic acid. At *m/z* resolving power of 400,000, ^{13}C-isotopologues of nucleotides were fully resolved from all other elemental isotopologues, thus allowing their ^{13}C fractional enrichment to be accurately determined. The method achieves both high sample and high information throughput analysis of nucleotides for metabolic pathway reconstruction in SIRM investigations.

Keywords Nucleotides · Stable isotope-resolved metabolomics (SIRM) · Direct-infusion · Simultaneous detection · FTICR MS · Ion-pair · ^{13}C-glucose · A549 · Methylseleninic acid

Abbreviations

AXP	Adenine nucleotides
FTICR-MS	Fourier transform ion cyclotron-mass spectrometry
HSQC	Heteronuclear single quantum coherence
MSA	Methylseleninic acid
PPP	Pentose phosphate pathway
PREMISE	Precalculated exact mass isotopologue search engine
SIRM	Stable isotope resolved metabolomics
THF	Tetrahydrofolate
UDP-GlcNAc	UDP-N-acetylglucosamine
UXP	Uracil nucleotides

1 Introduction

Nucleotides have a wide variety of essential functions in cells (Murray 2009; Nelson and Cox 2005). For example, the nucleoside triphosphates are the activated building

Electronic supplementary material The online version of this article (doi:10.1007/s11306-011-0388-y) contains supplementary material, which is available to authorized users.

P. Lorkiewicz · R. M. Higashi · T. W.-M. Fan (✉)
Department of Chemistry, University of Louisville, 2210 S. Brook St, Rm 348 John W. Shumaker Research Building, Louisville, KY 40292, USA
e-mail: twmfan@gmail.com

R. M. Higashi · A. N. Lane · T. W.-M. Fan
Center for Regulatory Environmental Analytical Metabolomics, 2210 S. Brook St, Louisville, KY 40292, USA

R. M. Higashi · A. N. Lane · T. W.-M. Fan
JG Brown Cancer Center, Clinical Translational Research Building, 505 S. Hancock St, Louisville, KY 40202, USA

blocks of nucleic acids, and energy drivers for anabolic metabolism via the hydrolysis of ATP and GTP. The nicotinamide and flavin nucleotides are critical cofactors in redox metabolism and energy production. The nucleotide hexoses are essential to the biosynthesis of complex carbohydrates and glycoproteins. Moreover, ATP, NAD^+, and nucleotide hexoses (e.g. UDP-N-acetylglucosamine) are respectively activated substrates for post-translational protein modification such as phosphorylation, ADP ribosylation, and O- and N-linked glycosylation, which regulate a wide variety of critical biological processes. Therefore, the ability to track nucleotide metabolism in cells or tissues is crucial to understanding cellular functions and regulations.

Although identification and quantification of metabolites are important elements of metabolomics analysis, measuring dynamic changes in metabolic networks such as synthesis and utilization of metabolites is indispensible to gaining insights into biochemical pathways and molecular regulation of metabolic networks. Such information can be acquired from stable isotope-resolved metabolomic (SIRM) studies (Fan et al. 2009; Lane et al. 2011, 2009; Moseley et al. 2011). In this approach, the incorporation of individual atoms of stable isotope-labeled tracers into multiple products is tracked simultaneously such that multiple metabolic pathways involved in the transformations can be reconstructed. Two analytical platforms have been used routinely for decades in tracer studies, i.e. NMR and mass spectrometry (MS). NMR is often the first choice for determining metabolite structures and their labeling patterns at specific atomic positions (positional isotopomers) (Fan et al. 2008, 2011b; Fan and Lane 2008). However, NMR is sometimes limited by sensitivity and resolution for detecting the labeled metabolites. MS and in particular the most recent Fourier transform-ion cyclotron resonance-MS (FTICR-MS) is complementary to NMR due to its higher sensitivity and superior ability to resolve and quantify mass isotopologues (differing by the number of labeled atoms) of labeled metabolites (Lane et al. 2008).

Chromatography-based MS methods for analyzing nucleotides have been reported in several studies. These approaches mainly coupled ion-pair reversed-phase (e.g. C_{18}) chromatography for nucleotide separation with MS detection (Coulier et al. 2006; Dodbiba et al. 2010; Lu et al. 2010). Commonly used ion pairing reagents (IPRs) such as tributylamine (Lu et al. 2010; Luo et al. 2007), hexylamine (HA) (Coulier et al. 2006) or organic di-/poly- cations (Dodbiba et al. 2010) are expected to interact with the phosphate group of nucleotides, thereby enhancing their affinity to the hydrophobic phase. IPRs that interact with nucleobase amino groups such as n-alkyl perfluorinated carboxylic acids have also been used for LC–MS separation (Feng et al. 2008). Other alternative LC–MS techniques are based on mixed-mode reversed-phase/weak anion exchange (Hinterwirth et al. 2010), hydrophilic interaction chromatography (Inoue et al. 2010) or affinity chromatography (Kammerer et al. 2005a, b). In addition to LC separations, capillary electrophoresis coupled to MS has also been used for detection of nucleotides (Soo et al. 2004).

Much less commonly described are methods for continuous-ion introduction MS analysis of nucleotides and nucleotide sugars in crude extracts. Such methods are required for obtaining the highest-quality isotopologue data, while affording higher sample throughput analysis. Past demonstrations were based on the use of a MALDI source coupled with time-of-flight (TOF) mass analyzers (Edwards and Kennedy 2005; Miura et al. 2010). The MALDI source suffers from rapidly changing ion yields, which is the same drawback as chromatographic inputs to a given ion source. Moreover, the ion sources were coupled to mass spectrometers with insufficient resolution to discriminate closely spaced isotopologue peaks of numerous labeled metabolites, which is typically required for SIRM studies.

In contrast, FTICR-MS is capable of sufficient resolution and accuracy for direct global analysis of labeled metabolites when run at a resolving power of 400,000. In addition, when coupled with nanoelectrospray ionization (nanoESI), such systems can deliver sufficiently stable ion yields with the bonus of small sample requirement, enhanced sensitivity, and high sample throughput, e.g. <5 min per sample. To date, continuous ion FTICR-MS methods for SIRM that detect lipids (Lane et al. 2009), amino acids (Pingitore et al. 2007), sugar nucleotides (Moseley et al. 2011) among others have been developed. However, a similar method for global nucleotide analysis in crude biological extracts has not been successful, at least in part due to ion suppression effects of the high salt (Annesley 2003) and/or complex matrix in crude extracts (Annesley 2003; Gangl et al. 2001; Matuszewski et al. 2003; Mei et al. 2003). Moreover, it has been difficult to establish stable nanoESI spray in untreated crude extracts (Higashi, Lorkiewicz unpublished).

To address these issues, we explored the ion pairing method by Coulier et al. 2006 developed for LC–MS analysis of nucleotides and other phosphorylated metabolites. Our method involves ion pairing of nucleotides in crude polar extracts with hexylamine before adsorption onto an embedded C_{18}-modified silica bed in 10 µl pipet tips, followed by elution with methanol. Those tips are routinely used in proteomics analyses for sample cleanup and desalting (Desiderio and Beranova-Giorgianni 2000; Pluskal 2000; Shukla and Majors 2005). This simple cleanup step sufficiently eliminated salt and matrix interference for subsequent continuous ion analysis by nanoESI FTICR-MS.

Here, we demonstrate the method using a mixture of 22 nucleotide standards and report the application of the method to the analysis of crude polar extracts of human adenocarcinoma A549 cells grown in uniformly ^{13}C-labeled glucose ([U-^{13}C] glucose) with or without methylseleninic acid (MSA, an anti-cancer selenium compound). We show not only the ability to fully resolve many nucleotides and their ^{13}C-isotopologues of less than 0.02 *m/z* difference, but also readily acquired changes in fractional ^{13}C enrichment of the latter in cancer cells in response to anti-cancer treatment.

2 Materials and methods

All nucleotide, nucleotide-sugars and other phosphorylated standards listed in Table 1, as well as glacial acetic acid, ammonia, ammonium acetate (NH_4Ac) and hexylamine (HA) were purchased from Sigma Aldrich (St. Louis, MO). Methanol was obtained from Burdick and Jackson (Morristown, NJ). Eighteen MΩ water was obtained using the ultrapure water system (Barnstead, Dubuque, IA). C_{18} tips (ZipTips) were purchased from Millipore (Billerica, MA).

2.1 Preparation of eluent reagents

Eluent reagents were prepared according to the procedure of Coulier et al. (2006). Briefly, Phase A consisted of 5 mM HA in H_2O with pH adjusted to 6.3 with acetic acid. Phase B consisted of 90% methanol and 10% 10 mM NH_4Ac adjusted to pH 8.5 with aqueous ammonia.

2.2 Preparation of the standard mixture

The nucleotide standards at 2.5 µM were prepared from 1 mM stock solutions in H_2O by diluting with methanol. 10 µl of the mixture was used for C_{18} tip processing according to the procedure described below.

2.3 Preparation of A549 extracts

Human lung adenocarcinoma A549 cells were grown on 10 cm plates in RPMI medium containing 10% fetal bovine serum, 100 U penicillin, 100 µg/ml streptomycin, 0.2% unlabeled or [U-^{13}C] labeled glucose, in the absence or presence of 5 µM MSA. The culture was incubated in 5% CO_2 at 37°C for 24 h as previously described (Fan et al. 2005). Next cells were washed three times in cold

Table 1 Relative intensity of metabolite peaks detected in a 2.5 µM nucleotide mixture before and after processing with C_{18} tip

Metabolite	Theoretical *m/z*	Unprocessed		C_{18} Processed	
		Mass accuracy error (ppm)	Relative intensity (%ATP)	Mass accuracy error (ppm)	Relative intensity (%ATP)
ATP	505.988478	0.5 ± 0.04	100 ± 0	0.56 ± 0.03	100 ± 0
ADP	426.022145	0.3 ± 0.06	117.23 ± 0.88	0.42 ± 0.04	100.64 ± 1.38
AMP	346.055812	0.5 ± 0.03	35.29 ± 0.44	0.73 ± 0.04	13.42 ± 0.44
cAMP	328.045247	0.55 ± 0.04	25.54 ± 0.21	0.7 ± 0.04	19.17 ± 0.37
CTP	481.977245	0.74 ± 0.06	67.53 ± 0.11	0.85 ± 0.03	67.69 ± 0.63
CDP	402.010912	0.76 ± 0.05	17.8 ± 0.17	0.95 ± 0.04	10.22 ± 0.2
CMP	322.044579	0.51 ± 0.05	13.19 ± 0.34	0.64 ± 0.04	2.29 ± 0.1
GTP	521.983393	0.61 ± 0.08	48.28 ± 0.09	0.75 ± 0.05	54.32 ± 0.28
GMP	362.050727	0.66 ± 0.03	21.55 ± 0.34	0.88 ± 0.03	5.16 ± 0.18
NAD	662.101853	0.95 ± 0.04	50.33 ± 3.09	1.51 ± 0.05	16.83 ± 0.54
NADH	664.117503	1.24 ± 0.1	9.78 ± 1.02	1.58 ± 0.08	10.54 ± 0.68
$NADP^+$	742.068186	0.76 ± 0.07	74.91 ± 3.74	0.76 ± 0.02	92.18 ± 2.73
NADPH	744.083836	1.37 ± 0.09	17.38 ± 0.82	1.5 ± 0.05	27.41 ± 0.72
UTP	482.961261	0.72 ± 0.08	69.62 ± 0.9	0.87 ± 0.04	66.3 ± 0.9
UDP	402.994928	0.5 ± 0.05	58.32 ± 1.34	0.76 ± 0.04	31.47 ± 0.67
UMP	323.028595	0.51 ± 0.03	13.49 ± 0.06	0.66 ± 0.04	3.24 ± 0.1
UDP-Glc[a]	565.047751	0.46 ± 0.05	98.54 ± 0.45	1.19 ± 0.05	27.24 ± 0.23
UDP-GNAc[a]	606.074302	0.34 ± 0.05	140.07 ± 2.12	1.22 ± 0.07	40.44 ± 0.39
GDP-Man[a]	604.069883	0.79 ± 0.08	62.28 ± 1.49	1.35 ± 0.07	23.93 ± 0.21
Ac-CoA[a]	808.118503	1.55 ± 0.1	13.41 ± 0.4	1.89 ± 0.09	5.63 ± 0.12
HEX-PP[a]	338.988778	0.59 ± 0.07	7.86 ± 0.22	0.75 ± 0.02	4.33 ± 0.1

The intensities were normalized to that of the ATP peak. Data were averaged from 3 traces

[a] *UDP-Glc* UDP-glucose; *UDP-GNAc* UDP-*N*-acetyl-glucosamine; *GDP-Man* GDP-mannose; *Ac-CoA* acetyl-CoA; *HEX-PP* hexose-bis-phosphate

PBS before cell metabolism was quenched and cell lysed by 1 ml ice cold acetonitrile (ACN) (adapted from Fan et al. 2011a). 18 MΩ water (0.75 ml) was added to the lysed cells, which were harvested with a cell scraper before transferring into 15 ml polypropylene conical centrifuge tubes (Sarstedt). This process was repeated once. Chloroform (1 ml, HPLC grade, Fisher Scientific) and 3 mm diameter glass beads were added to the cell lysates, which were shaken rigorously to extract lipids into the chloroform layer while precipitating proteins. The final ACN:H_2O:chloroform ratio was 2:1.5:1. The extract mixture was centrifuged at 3,500×*g* for 20 min at 4°C to yield the polar and non-polar extracts in the top and bottom layers, respectively, and the protein precipitates in the interface. The polar extracts were then lyophilized (Fan 2010) and dissolved in 100% phase A. 10 µl (about 5% of the total extract, corresponding to $<3 \times 10^5$ cells) was then used for C_{18} tip processing.

2.4 Sample processing through C_{18} Tips

The C_{18} tip was first conditioned by washing it five times in methanol and then 5 times in 100% Phase A. The 10 µl aliquot was then loaded onto the tip through a series of eight aspirations, followed by washing in 10 µl of 100% phase A with 4 aspirations. In the elution step, the tip was aspirated in 10 µl of 70% phase A and 30% of phase B for 8–12 times. This process was repeated with another 10 µl of the same eluent to ensure complete elution of nucleotides. The combination of 70% Phase A and 30% Phase B was found to provide the best elution conditions and nanoESI spray stability. Higher fractions of Phase B allowed for complete elution without the additional rinse with the eluent but the higher solution pH resulted in the formation of several sodium adducts, leading to increased spectral complexity. Furthermore, higher Phase B in the eluent buffer led to a peak in the FTICR-MS spectra with an accurate mass corresponding to NAD^+ minus nicotinamide (putatively assigned as cyclic-ADPribose—$[C_{15}H_{21}N_5O_{13}P_2\text{-}H]^-$), which suggests the loss of the nicotinamide ring and cyclization, possibly via pH-induced decomposition. Finally the tip was washed with 100% methanol to elute any remaining metabolites. This step was not essential as no nucleotide peaks were routinely detected in this fraction (spectra not shown). The nucleotide fraction was then diluted three-fold with 100% methanol to ensure stable spray conditions for analysis. Interestingly, if 100% MeOH (usually an excellent nanoESI spray solvent) was used for elution instead of 70% Phase A, the spray current fluctuated considerably and eventually failed which made it difficult to acquire spectra for longer than ca. 2 min. With the optimized method as described, a spray stable for >15 min was achievable, and was readily adapted for multiple sample processing using a 96-well PCR plate and a multichannel or robotic pipettor. An added advantage of using microtiter plates is the dual purpose of sample processing/storage and compatibility with automated sample delivery for analysis.

2.5 FTICR-MS analysis

All samples were analyzed by continuous infusion into a 7 Tesla hybrid LTQ® ion trap–FTICR mass spectrometer (LTQ–FT, Thermo Finnigan, Bremen, Germany) equipped with a Triversa Nanomate nanoESI ion source (Advion Biosciences, Ithaca, NY). Data were acquired in the negative ion mode. The instrument was calibrated according to manufacturer protocols and tuned using the $[ATP\text{-}H]^-$ peak (theoretical $m/z = 505.988478$ Da). The Triversa Nanomate was operated at 1.5 kV and 0.5 psi head pressure using the "A" chip (5.5 µm nozzle), which yielded the most stable spray conditions. To monitor the stability of the spray and ion delivery, FTICR-MS scans were preceded by a 30 s low-resolution ion trap (LTQ) scan. The FTICR-MS traces were acquired in mass range from 250 Da to 800 Da with a target mass resolving power set to 400,000 at 400 *m/z* and the target resolution was achieved effectively. The maximum ion time for the automatic gain control (AGC) was set to 1,000 ms (typically <10 ms was used) using default AGC targets. Five transients were summed to produce each transformed mass spectrum, resulting in a cycle time for each stored spectrum of about 10 s (2 s per transient). A sample run was completed in 5 min for the standard mixture and 15 min for A549 cell extracts to obtain sufficient ion counts for low-abundance isotopologue peaks. This amounted to a total of 30 or 90 saved spectra that were then co-added to produce a final spectrum. The effective width at half height of the spectral peaks was about 1.5×10^{-3} Da (mDa), indicating that peaks that differ in mass greater than this limit (e.g. ^{13}C, ^{15}N, and ^{2}H) can be resolved under these conditions (cf. Fig. 3a, d).

High-resolution spectral profile data were visualized using the Xcalibur software (Thermo Electron, ver. 2 SP2 FT) and the exact *m/z* values and peak intensities obtained in the centroid mode were exported as a spreadsheet file. The metabolite species were assigned using an in-house software PREMISE (PRecaculated Exact Mass Isotopologue Search Engine) (Lane et al. 2009) by matching the experimental *m/z* values against a list of the theoretical *m/z* values. Matching criteria with an *m/z* window of 0.0022 *m/z* or smaller was sufficient to assign most monoisotopic peaks of nucleotides. Natural abundance stripping was carried out using the protocol developed by Moseley (2010) using the equations:

$$I_{M+i} = \frac{I_{M+i;\mathrm{NA}} - \sum_{x=0}^{x<i} I_{M+x} * B_C(x,i)}{1 - B_C\mathrm{sum}(i)} \quad (1)$$

$$B_{c|}(n,k) = \binom{C_{\mathrm{Max}} - n}{k - n} (1 - \mathrm{NA}_{13_c})^{C_{\mathrm{Max}}-k} \mathrm{NA}_{13_C}^{k-n} \quad (2)$$

where NA is natural abundance (1.07% for ^{13}C), k is the total number of carbons and n is the number of ^{13}C atoms.

This iterative procedure was shown to provide good results on a variety of species including lipids and sugar nucleotides (Lane et al. 2009; Moseley et al. 2011). The residual error associated with the stripping depends on signal-to noise ratios, but typically reduces the NA contribution by an order of magnitude or better, as shown here as tests on unlabeled nucleotides, where the $m_0 + 1$ peak was reduced from 10 to 0.00%.

3 Results and discussion

3.1 Analysis of standards

The sample processing method was first evaluated using a mixture of 22 standards comprising common ribonucleotides, nucleotide sugars, sugar phosphates and acetyl-CoA. These metabolites are important in numerous cellular functions and are difficult to detect by electrospray MS in crude extracts without prior separation. The standard mixture was processed with a C_{18} tip and both the eluates and unprocessed standards were analyzed by FTICR-MS. Figure 1 compares the FTICR-MS traces acquired on a 2.5 μM standard mixture before and after processing with the C_{18} tip. The peak assignments are summarized in Table 1, where the peak intensities were normalized to that of $[ATP–H]^-$ ($m/z = 505.988478$). It is clear that all standards were recovered from the C_{18} tip processing but the original peak ratios were not fully preserved (Figure S1). For example, the intensity of the UDP-GlcNAc peak after C_{18} tip processing was about one-third of that without processing.

Although not all standards were fully recovered in the C_{18} tip eluates, the elution profile was reproducible from sample-to-sample as observed in Figure S1. This suggests that absolute quantification of individual nucleotides can be achieved with the addition of internal standards. However, quantitative analysis of isotopologue distributions is independent of the recovery shortfall or interference of the sample matrix, because each isotopologue intensity is normalized against the intensity sum of all isotopologues to obtain fractional distribution. Therefore, no internal standards are necessary for obtaining fractional distribution of nucleotide isotopologues, which is arguably the most important data parameter for SIRM studies (Fan et al. 2009; Lane et al. 2008, 2011; Moseley et al. 2011). This advantage is fortuitously convenient since authentic standards of every possible metabolite isotopologues are simply unavailable.

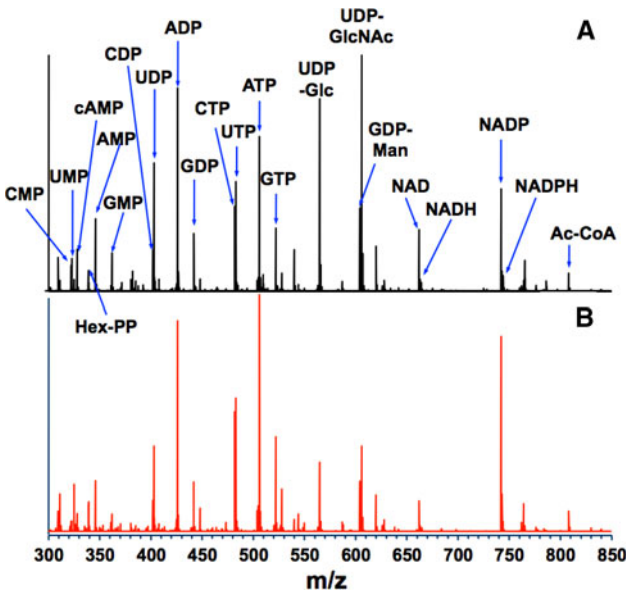

Fig. 1 FTICR-MS spectra of nucleotide standards Traces were acquired on a 2.5 μM mixture of 22 standards comprising: ATP, ADP, AMP, cAMP, CTP, CDP, CMP, GTP, GDP, GMP, NAD^+, $NADP^+$, NADH, NADPH, UTP, UDP, UMP, UDPG, UDPGNAc, GDP-mannose, Ac-CoA (acetyl CoA), fructose 1,6 bisphosphate (Hex-PP) as described in the Methods. **a**, **b** represent respectively before and after processing with the C_{18} tip

3.2 Analysis of nucleotides in unlabeled polar extracts of A549 cells

We have initially attempted analysis of polar extracts of unlabeled A549 cells by nanoESI FTICR-MS without processing through the C_{18} tip. Upon infusion, the nanoESI current decayed immediately and no usable acquisitions were obtained. When the same crude extract was processed using C_{18} tip, the nanoESI current was stable for >5 min, which enabled nucleotides and numerous other metabolite (e.g. glutathione, acetyl CoA, sugar phosphates, cf. Fig. 1) peaks to be readily observed. Figure 2 shows a representative negative-ion mode spectrum of an A549 extract after C_{18} tip processing. The major nucleotides and nucleotide sugars were clearly detected in extracts, along with low abundance nucleotides such as NADH, $NADP^+$, UMP, and GMP.

3.3 Analysis of nucleotides and ^{13}C-isotopologue distribution in labeled A549 extracts

As stated above, SIRM experiments are necessary to track accurately changes in metabolic networks and fluxes. We

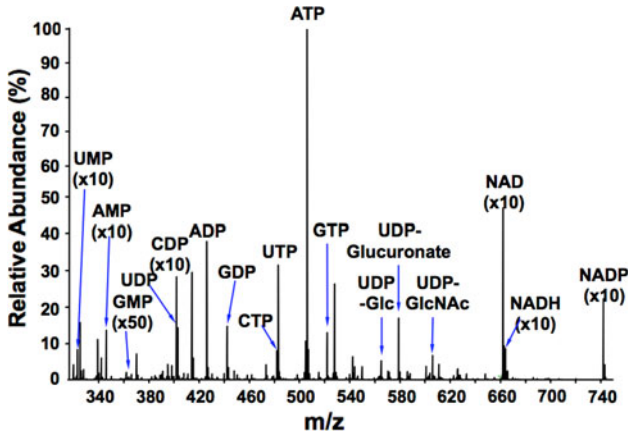

Fig. 2 Typical negative ion mode spectrum of A549 polar extract after processing with C_{18} tip. The peak assignments were made using "PREMISE" (Lane et al. 2009) and vetted manually. All common nucleotides, nucleotide sugars and other phosphorylated metabolite shown represent deprotonated species

conducted such an experiment with A549 cells grown in [U-^{13}C]-glucose for 24 h for comparison with cells grown in unlabeled glucose. Figure 3 shows the CTP/UTP (panels A, B) and ATP (panels D, E) regions of the spectral traces acquired from the polar extracts of labeled versus unlabeled A549 cells. Also shown as expanded regions is the clear resolution of $^{15}N_1$, $^{13}C_1$, and $^{2}H_1$ isotopologues of UTP (panel A) and ATP (panel D) at natural abundance, which differ by 6 and 3.1 mDa, respectively. The widths at half height of these peaks were ca. 1.5 mDa, which was more than adequate to resolve the three isotopologue peaks for both nucleotides.

The labeled spectral traces (B, E) had a dramatically different appearance from the unlabeled traces (A, D) for both the pyrimidine and the purine nucleotides. All ^{13}C isotopologue peaks were assigned using PREMISE based on their accurate mass values, which differed from that of the respective monoisotopic species by incremental neutron (instead of proton) mass values. Thus, extensive ^{13}C labeling was evident for all observable nucleotides (Fig. 3b, e and data not shown) and up to eight ^{13}C atoms were present in UTP and ATP. It is also notable in Fig. 3b, e that most of the monoisotopic peaks were depleted while the most intense isotopologue peak in all cases was the $^{13}C_5$ species ($m_0 + 5$). The expected origins of the ^{13}C atoms in the purine and pyrimidine isotopologues are depicted in their respective biosynthetic pathways in Fig. 3c, f.

The fractional ^{13}C enrichment in the various isotopologues of four selected purine and pyrimidine nucleotides was calculated from respective peak intensity and summarized in Fig. 4. These enrichment values were obtained by stripping natural abundance ^{13}C contribution from each of the isotopologues for singly to multiply-labeled species, using the protocol developed by Moseley (2010). We have previously shown that at high signal-to noise ratios, the isotope ratio accuracy for lipids is 1% or better (Lane et al. 2009). The accuracy and precision for the determination of relative distribution of nucleotide isotopologues at natural abundance is illustrated in Table S1 (Supplementary Materials). The isotope ratio accuracy achieved for the $m_0 + 1$ isotopologue was 0.2–2.4%, comparable to the previous findings.

After 24 h of labeling, only $\leq$12% of the m_0 peak (the all-^{12}C species) remained, although the total nucleotide concentration did not change significantly over this period (from ^{1}H NMR data, not shown). Therefore, the existing nucleotide pool was replaced by newly synthesized nucleotides, using externally supplied $^{13}C_6$-glucose. The dominant fraction was the $m_0 + 5$ or $^{13}C_5$ isotopologue (>69%), which was comparable among the four selected nucleotides. This isotopologue is attributable to the $^{13}C_5$ ribose substructure of each nucleotide (Fig. 3c, f), with no label in the nucleobase. This is consistent with extensive cross-validation by NMR, FTICR-MS, and computational modeling (Fan and Lane 2011; Moseley et al. 2011).

The incorporation of $^{13}C_5$-ribose into nucleotides from [U-^{13}C]-glucose implicates the activity of hexose kinase and the pentose phosphate pathway (PPP). Other significant isotopologues, $m_0 + 6$, $m_0 + 7$ and $m_0 + 8$ represent simultaneous incorporation of glucose carbon into the nucleobase and ribose subunits. Here the purines and pyrimidines behave differently, reflecting their different metabolic pathways (Fan et al. 2008; Murray et al. 2009). The pyrimidine bases are synthesized from aspartate and CO_2 (an unlabeled source) (Fig. 3c). Aspartate can be labeled from ^{13}C-glucose through the sequence of glycolysis and the Krebs cycle, which results in a mixture of singly to triply ^{13}C-labeled Asp (Fan et al. 2011a, b). Labeled Asp can in turn be incorporated into pyrimidine bases, leading to the production of $m_0 + 6$ ($^{13}C_6$) to $m_0 + 8$ ($^{13}C_8$) isotopologues of pyrimidine nucleotides with the base attached to a $^{13}C_5$ labeled ribose subunit. In contrast, purine synthesis utilizes carbon from glycine, CO_2 and N^{10}-formyl-tetrahydrofolate (N^{10}-formyl-THF). Glycine can be synthesized from glucose via the 3-phosphoglycerate/serine pathways, which also lead to the production of N^{10}-formyl-THF (Fig. 3f). Therefore, [U-^{13}C]-glucose conversion to ribose, glycine and N^{10}-formyl-THF is expected to produce the $^{13}C_6$ to $^{13}C_8$ isotopologues of purine nucleotides. The higher fractional ^{13}C enrichment in these isotopologues of the purine nucleotides, as compared to those of the pyrimidine nucleotides, suggests a higher extent of de novo synthesis of purine than pyrimidine rings in A549 cells. This behavior is not previously known, to the best of our knowledge. It could reflect a higher turnover demand (e.g. ADP ribosylation) for purine than pyrimidine nucleotides.

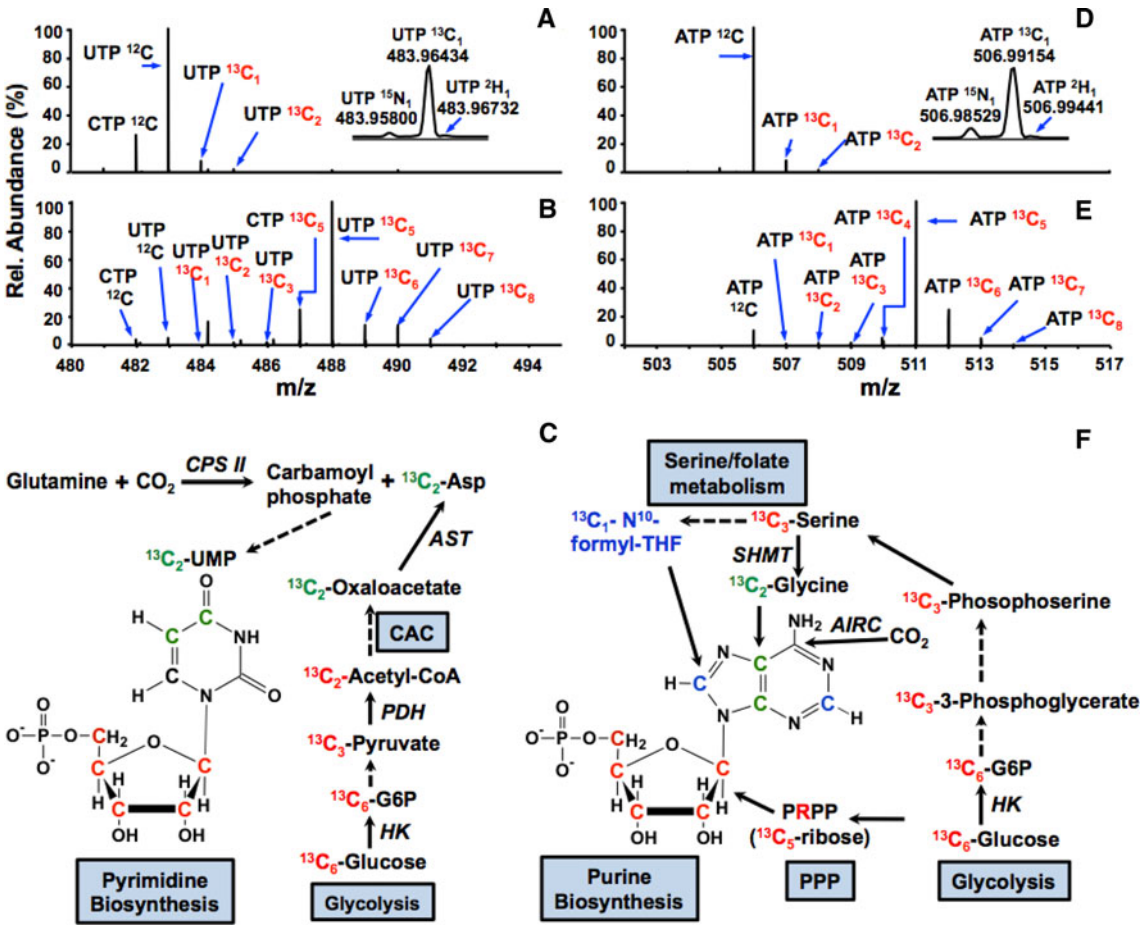

Fig. 3 ^{13}C-Isotopologue distributions in ATP, UTP, and CTP present in a polar extract of A549 cells A549 cells were grown for 24 h in the presence of [U-^{13}C]-glucose and the metabolites were extracted and pre-processed with C18 tip before FTICR-MS analysis, as described in Sect. 2. FTICR-MS spectral regions of UTP, CTP, and ATP are shown. **a** UTP and CTP (unlabeled) with an insert showing the resolution of ^{15}N, ^{13}C, and ^{2}H isotopologues of UTP at natural abundance. **b** UTP and CTP (^{13}C labeled); **c** Pyrimidine biosynthesis pathway. The ribose moiety is derived from the pentose phosphate pathway (PPP), and the pyrimidine base is synthesized in separate pathways from aspartate and CO_2. Illustrated in **c** is the uracil ring with ^{13}C labeled at C4 and C5 positions, which is derived from $^{13}C_2$-3,4-Asp produced from $^{13}C_6$-glucose after the first turn of the citric acid cycle (CAC). Due to metabolic scrambling via CAC, the ^{13}C-6-uracil isotopologue is also produced, which is derived from $^{13}C_2$-1,2-Asp (not shown) (Fan et al. 2010). **d** ATP (unlabeled) with an insert showing the resolution of ^{15}N, ^{13}C, and ^{2}H isotopologues of ATP at natural abundance; **e** ATP (^{13}C labeled); F. Purine biosynthesis pathway. The purine base is built directly on the ribose moiety using CO_2, glycine, glutamine and N^{10}-formyl tetrahydrofolate (THF). The atoms in the purine and pyrimidine bases are color-coded with their synthetic precursors, e.g. C's in uracil ring are derived from Asp. *CPS II* Carbamoyl phosphate synthetase II; *AST* aspartate aminotransferase; *PDH* pyruvate dehydrogenase; *HK* hexose kinase; *AIRC* phosphoribosyl aminoimidazole carboxylase; *SHMT* serine hydroxymethyltransferase; single step reaction (*solid arrows*); multi-step reactions (*dashed arrows*)

We have also shown previously that the rates of synthesis of ribose moieties of nucleotides differ between pyrimidines and purines in other systems (Fan et al. 2008). These examples illustrate how intersecting metabolic pathways can be reconstructed from SIRM analysis of nucleotides (Moseley et al. 2011) utilizing the method described in this paper.

3.4 MSA altered nucleotides biosynthesis in A549 cells

We then applied the method to analyze the changes in nucleotide biosynthesis in A549 cancer cells induced by 5 μM MSA, a cytotoxic selenium compound. A549 cells were grown in [U-^{13}C]-glucose for 24 h with or without MSA. FTICR-MS spectra were recorded for the polar extracts after C_{18} tip cleanup as described above. The spectral traces shown side-by-side in Figure S2 reveal clear differences in the labeling patterns of ATP (panels A, B), UTP, and CTP (panels C, D) between control and MSA treatments. The ^{13}C fractional distributions of various isotopologues of ATP and UTP were calculated from their peak intensity after natural abundance stripping, and are compared in Fig. 5. For ATP, relative to the dominant m + 5 isotopologue ($^{13}C_5$-ribose), the all ^{12}C or m_0

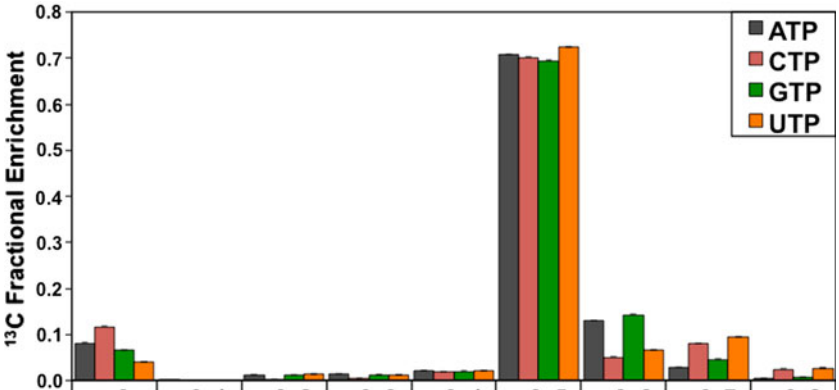

	m0	m0+1	m0+2	m0+3	m0+4	m0+5	m0+6	m0+7	m0+8
ATP	0.08	0.00	0.01	0.01	0.02	0.71	0.13	0.03	0.00
CTP	0.12	0.00	0.00	0.00	0.02	0.70	0.05	0.08	0.03
GTP	0.07	0.00	0.01	0.01	0.02	0.69	0.14	0.05	0.01
UTP	0.04	0.00	0.01	0.01	0.02	0.72	0.07	0.09	0.03

Fig. 4 Fractional ^{13}C isotopologue enrichment of ATP, CTP, GTP and UTP in [U-^{13}C]-glucose labeled A549 polar extract A549 cells were grown in [U-^{13}C]-glucose, extracted, processed, and analyzed as in Fig. 3. Mass isotopologues were assigned as described in Sect. 2 and natural abundance contribution was stripped using the routine described by Moseley (2010). The fractional enrichment bar graph and the values listed in the table below was calculated by dividing individual isotopologue intensity by the sum of all isotopologue intensities. *Error bars* represent standard error ($n = 4$)

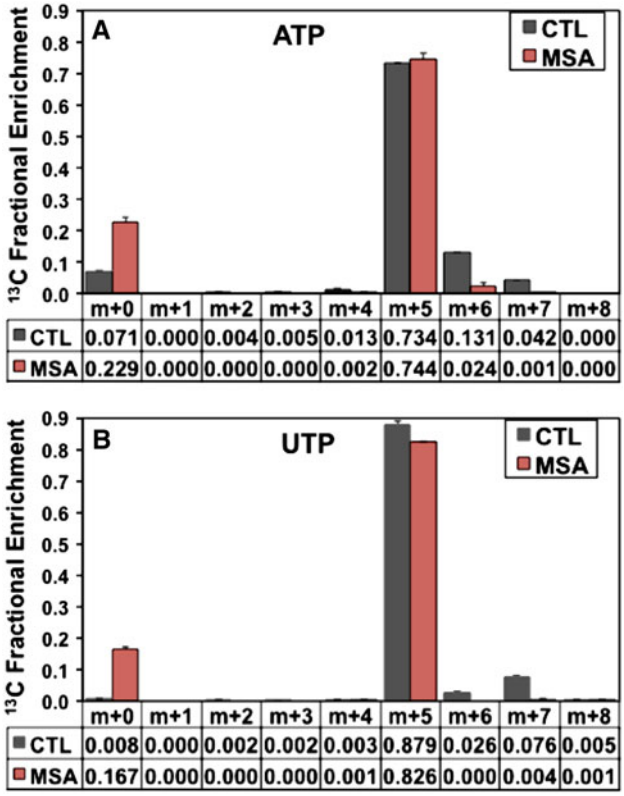

	m+0	m+1	m+2	m+3	m+4	m+5	m+6	m+7	m+8
CTL	0.071	0.000	0.004	0.005	0.013	0.734	0.131	0.042	0.000
MSA	0.229	0.000	0.000	0.000	0.002	0.744	0.024	0.001	0.000

	m+0	m+1	m+2	m+3	m+4	m+5	m+6	m+7	m+8
CTL	0.008	0.000	0.002	0.002	0.003	0.879	0.026	0.076	0.005
MSA	0.167	0.000	0.000	0.000	0.001	0.826	0.000	0.004	0.001

Fig. 5 Effect of MSA on distributions of ^{13}C-isotopologue of nucleotides in polar extract of A549 cells Cells were grown in [U-^{13}C]-glucose with or without MSA, extracted, processed, and analyzed as in Fig. 3. *Bar charts* and table below depict fractional ^{13}C enrichment in the isotopologue of ATP (**a**) and UTP (**b**). The fractional enrichment was calculated by dividing individual isotopologue intensity by the sum of all isotopologue intensities. *Error bars* represent standard error ($n = 2$)

fraction was ca. three fold higher in the MSA-treated (~23%) than in untreated cells (~7%) (Fig. 5a). In contrast, the fractions of the $m_0 + 6$, $m_0 + 7$, and $m_0 + 8$ isotopologues ($^{13}C_{1-3}$-nucleobase + $^{13}C_5$-ribose) of the MSA-treated cells were significantly reduced in comparison with the untreated sample. Moreover, the total ^{13}C abundance of the ribosyl unit of adenine nucleotides (AXP) decreased significantly by the MSA treatment, as evidenced from the 1-D ^{13}C-filtered ^{1}H HSQC NMR analysis (Figure S2E). Altogether, these data indicate that MSA substantially inhibited purine nucleotide biosynthesis. The effect of MSA on pyrimidine labeling patterns was even more dramatic, as shown in Fig. 5 and S2C-E. In the untreated cells, the all ^{12}C or m + 0 peak of UTP constituted < 1% of the total intensity, whereas in the presence of MSA, this fraction was 17% (Fig. 5b). Furthermore, the loss of $m_0 + 6$ to $m_0 + 8$ ($^{13}C_6$ to $^{13}C_8$) isotopologue fractions of UTP indicates that 5 μM MSA almost completely suppressed de novo biosynthesis of the pyrimidine rings in A549 cells, in addition to the inhibition of ribosyl synthesis (cf. uracil nucleotides (UXP) and their sugar derivatives in Figure S2E) (Fan et al. 2011b). These effects on nucleotide biosynthesis may underlie MSA's ability to inhibit cancer cell growth (Fan et al. 2011b).

4 Conclusions

We have developed a rapid and comprehensive high information throughput analysis for nucleotides and other

polar phosphorylated metabolites by continuous infusion FTICR-MS. This method coupled ion pairing between phosphate groups and hexylamine with C_{18} tip-based cleanup to enable 5–15 min FTICR-MS analysis of phosphorylated metabolites down to nanomolar levels in crude cell extracts. Absolute quantification may require the use of internal standards due to a variable recovery of different nucleotides from the cleanup procedure. Most importantly, the method is excellently suited for the crucial parameter for SIRM, i.e., relative quantification of ^{13}C isotopologue distribution of nucleotides biosynthesized from ^{13}C-labeled tracers. This was demonstrated for lung cancer A549 cells grown in $^{13}C_6$-glucose tracer. The labeling patterns of nucleotides enabled the reconstruction of the intersecting metabolic pathways involved. These data may be further mined for multi-pathway flux modeling, using the recently developed GAIMS algorithm (Moseley et al. 2011). We also illustrated the utility of the method for probing perturbations in nucleotide biosynthesis induced by an anticancer selenium agent. The method is generally applicable to other cell and tissue extracts.

Acknowledgments We thank R. Burra and T. Xu for technical assistance, H. Moseley for valuable discussions, and J. Winnike for critical comments on the manuscript. This study was supported in part by NIH Grant numbers 1R01CA118434-01A2, 3R01CA118434-02S1, Kentucky Lung Cancer Research Program (LCRP) OGMB101380 (to TWMF), 1R21CA133668-01A2 (to ANL), University of Louisville CTSPGP grant numbers 20044 (to TWMF) and 20061 (to ANL), and Kentucky Lung Cancer Research Program (postdoctoral fellowship to PL). The FTICR-MS instrumentation was supported by NSF/EPSCoR grant number EPS-0447479 (TWMF).

References

Annesley, T. M. (2003). Ion suppression in mass spectrometry. *Clinical Chemistry, 49*, 1041–1044.

Coulier, L., Bas, R., Jespersen, S., Verheij, E., van der Werf, M. J., & Hankemeier, T. (2006). Simultaneous quantitative analysis of metabolites using ion-pair liquid chromatography: Electrospray ionization mass spectrometry. *Analytical Chemistry, 78*, 6573–6582.

Desiderio, D. M., & Beranova-Giorgianni, S. (2000). Mass spectrometry of the human pituitary proteome: Identification of selected proteins. *Rapid Communications in Mass Spectrometry, 14*, 161–167.

Dodbiba, E., Breitbach, Z. S., Wanigasekara, E., Payagala, T., Zhang, X. T., & Armstrong, D. W. (2010). Detection of nucleotides in positive-mode electrospray ionization mass spectrometry using multiply-charged cationic ion-pairing reagents. *Analytical and Bioanalytical Chemistry, 398*, 367–376.

Edwards, J. L., & Kennedy, R. T. (2005). Metabolomic analysis of eukaryotic tissue and prokaryotes using negative mode MALDI time-of-flight mass spectrometry. *Analytical Chemistry, 77*, 2201–2209.

Fan, T. W.-M. (2010). Metabolomics-edited transcriptomics analysis (Meta). In C. A. McQueen (Ed.), *Comprehensive toxicology* (pp. 685–706). Oxford: Academic Press.

Fan, T. W.-M., & Lane, A. N. (2008). Structure-based profiling of Metabolites and isotopomers by NMR. *Progress in NMR Spectroscopy, 52*, 69–117.

Fan, T. W.-M., & Lane, A. N. (2011). NMR-based stable isotope resolved metabolomics in systems biochemistry. *Journal of Biomolecular NMR, 49*, 267–280.

Fan, T., Bandura, L., Higashi, R., & Lane, A. (2005). Metabolomics-edited transcriptomics analysis of Se anticancer action in human lung cancer cells. *Metabolomics Journal, 1*, 325–339.

Fan, T. W.-M., Kucia, M., Jankowski, K., Higashi, R. M., Ratacjak, M. Z., Ratacjak, J., et al. (2008). Proliferating Rhabdomyosarcoma cells shows an energy producing anabolic metabolic phenotype compared with primary myocytes. *Molecular Cancer, 7*, 79.

Fan, T. W., Lane, A. N., Higashi, R. M., Farag, M. A., Gao, H., Bousamra, M., et al. (2009). Altered regulation of metabolic pathways in human lung cancer discerned by ^{13}C stable isotope-resolved metabolomics (SIRM)). *Molecular Cancer, 8*, 41.

Fan, T. W.-M., Yuan, P., Lane, A. N., Higashi, R. M., Wang, Y., Hamidi, A., et al. (2010). Stable isotope-resolved metabolomic analysis of lithium effects on glial-neuronal metabolism and interactions. *Metabolomics, 6*, 165–179.

Fan, T. W.-M., Lane, A. N., Higashi, R. M., & Yan, J. (2011a). *Stable isotope resolved metabolomics of lung cancer in a SCID mouse model metabolomics, 7*, 257–269.

Fan, T. W.-M., Tan, J. L., McKinney, M. M., & Lane, A. N. (2011b) Stable isotope resolved metabolomics analysis of ribonucleotide and rna metabolism in human lung cancer cells. *Metabolomics* doi:10.1007/s11306-011-0337-9.

Feng, H. T., Wong, N., Wee, S., & Lee, M. M. (2008). Simultaneous determination of 19 intracellular nucleotides and nucleotide sugars in Chinese Hamster ovary cells by capillary electrophoresis. *Journal of Chromatography B-Analytical Technologies in the Biomedical and Life Sciences, 870*, 131–134.

Gangl, E. T., Annan, M., Spooner, N., & Vouros, P. (2001). Reduction of signal suppression effects in ESI-MS using a nanosplitting device. *Analytical Chemistry, 73*, 5635–5644.

Hinterwirth, H., Lammerhofer, M., Preinerstorfer, B., Gargano, A., Reischl, R., Bicker, W., et al. (2010). Selectivity issues in targeted metabolomics: Separation of phosphorylated carbohydrate isomers by mixed-mode hydrophilic interaction/weak anion exchange chromatography. *Journal of Separation Science, 33*, 3273–3282.

Inoue, K., Obara, R., Hino, T., & Oka, H. (2010). Development and application of an HILIC-MS/MS method for the quantitation of nucleotides in infant formula. *Journal of Agricultural and Food Chemistry, 58*, 9918–9924.

Kammerer, B., Frickenschmidt, A., Gleiter, C. H., Laufer, S., & Liebich, H. (2005a). MALDI-TOF MS analysis of urinary nucleosides. *Journal of the American Society for Mass Spectrometry, 16*, 940–947.

Kammerer, B., Frickenschmidt, A., Muller, C. E., Laufer, S., Gleiter, C. H., & Liebich, H. (2005b). Mass spectrometric identification of modified urinary nucleosides used as potential biomedical markers by LC-ITMS coupling. *Analytical and Bioanalytical Chemistry, 382*, 1017–1026.

Lane, A. N., Fan, T. W., & Higashi, R. M. (2008). Isotopomer-based metabolomic analysis by NMR and mass spectrometry. *Biophysical Tools for Biologists, 84*, 541–588.

Lane, A. N., Fan, T. W.-M., Xie, X., Moseley, H. N., & Higashi, R. M. (2009). Stable isotope analysis of lipid biosynthesis by high resolution mass spectrometry and NMR. *Analytica Chimica Acta, 651*, 201–208.

Lane, A. N., Fan, T. W.-M., Bousamra, M., I. I., Higashi, R. M., Yan, J., & Miller, D. M. (2011). Clinical applications of stable isotope-resolved metabolomics (SIRM) in non-small cell lung cancer. *Omics, 15*, 173–182.

Lu, W. Y., Clasquin, M. F., Melamud, E., Amador-Noguez, D., Caudy, A. A., & Rabinowitz, J. D. (2010). Metabolomic analysis via reversed-phase ion-pairing liquid chromatography coupled to a stand alone orbitrap mass spectrometer. *Analytical Chemistry, 82*, 3212–3221.

Luo, B., Groenke, K., Takors, R., Wandrey, C., & Oldiges, M. (2007). Simultaneous determination of multiple intracellular metabolites in glycolysis, pentose phosphate pathway and tricarboxylic acid cycle by liquid chromatography-mass spectrometry. *Journal of Chromatography. A, 1147*, 153–164.

Matuszewski, B. K., Constanzer, M. L., & Chavez-Eng, C. M. (2003). Strategies for the assessment of matrix effect in quantitative bioanalytical methods based on HPLC-MS/MS. *Analytical Chemistry, 75*, 3019–3030.

Mei, H., Hsieh, Y. S., Nardo, C., Xu, X. Y., Wang, S. Y., Ng, K., et al. (2003). Investigation of matrix effects in bioanalytical high-performance liquid chromatography/tandem mass spectrometric assays: application to drug discovery. *Rapid Communications in Mass Spectrometry, 17*, 97–103.

Miura, D., Fujimura, Y., Tachibana, H., & Wariishi, H. (2010). Highly sensitive matrix-assisted laser desorption ionization-mass spectrometry for high-throughput metabolic profiling. *Analytical Chemistry, 82*, 498–504.

Moseley, H. N. (2010). Correcting for the effects of natural abundance in stable isotope resolved metabolomics experiments involving ultra-high resolution mass spectrometry. *BMC Bioinformatics, 11*, 139.

Moseley, H. N. B., Lane, A. N., Belshoff, A. C., Higashi, R. M., & Fan, T. W.-M. (2011). Non-steady state modeling of UDP-GlcNAc biosynthesis is enabled by stable isotope resolved metabolomics (SIRM). *BMC Biology, 9*, 37.

Murray, K. M. (2009). *Glycoproteins, Harper's Illustrated Biochemistry*. New York: McGraw-Hill.

Murray, R. K., Bender, D. A., Botham, K. M., Kennelly, P. J., Rodwell, V. W., & Weil, P. A. (2009). *Harper's Illustrated Biochemistry*. New York: McGraw-Hill.

Nelson, D. L., & Cox, M. M. (2005). *Lehninger principles of biochemistry* (4th ed.). New York: W.H. Freeman and Company.

Pingitore, F., Tang, Y. J., Kruppa, G. H., & Keasling, J. D. (2007). Analysis of amino acid isotopomers using FT-ICR MS. *Analytical Chemistry, 79*, 2483–2490.

Pluskal, M. G. (2000). Microscale sample preparation. *Nat Biotech, 18*, 104–105.

Shukla, A. & Majors, R. E. (2005) Micropipette tip-based sample preparation for bioanalysis. *Lc Gc North America 23,* 646.

Soo, E. C., Aubry, A. J., Logan, S. M., Guerry, P., Kelly, J. F., Young, N. M., et al. (2004). Selective detection and identification of sugar nucleotides by CE-electrospray-MS and its application to bacterial metabolomics. *Analytical Chemistry, 76*, 619–626.